Bulky Adamantanethiolate and Cyclohexanethiolate Ligands Favor Smaller Gold Nanoparticles with Altered Discrete Sizes

Peter J. Krommenhoek,[†] Junwei Wang,[†,⊥] Nathaniel Hentz,[‡] Aaron C. Johnston-Peck,[†] Krystian A. Kozek,[†] Gregory Kalyuzhny,[§] and Joseph B. Tracy[†,*]

[†]Department of Materials Science and Engineering and [‡]Biomanufacturing Training and Education Center, North Carolina State University, Raleigh, North Carolina 27695, United States and [§]Department of Chemistry and Biochemistry, San Diego State University, San Diego, California 92182, United States. [⊥]Present address: Department of Materials Science and Engineering, Rensselaer Polytechnic Institute, Troy, NY 12180.

ABSTRACT

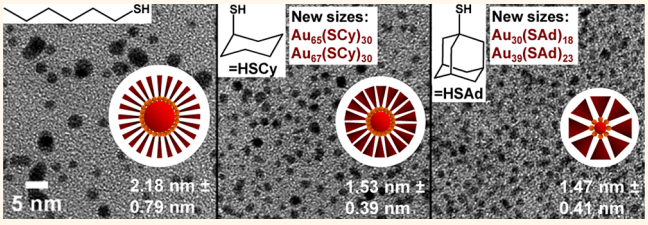

Use of bulky ligands (BLs) in the synthesis of metal nanoparticles (NPs) gives smaller core sizes, sharpens the size distribution, and alters the discrete sizes. For BLs, the highly curved surface of small NPs may facilitate growth, but as the size increases and the surface flattens, NP growth may terminate when the ligand monolayer blocks BLs from transporting metal atoms to the NP core. Batches of thiolate-stabilized Au NPs were synthesized using equimolar amounts of 1-adamantanethiol (AdSH), cyclohexanethiol (CySH), or *n*-hexanethiol (C6SH). The bulky CyS- and AdS-stabilized NPs have smaller, more monodisperse sizes than the C6S-stabilized NPs. As the bulkiness increases, the near-infrared luminescence intensity increases, which is characteristic of small Au NPs. Four new discrete sizes were measured by MALDI-TOF mass spectrometry, $Au_{30}(SAd)_{18}$, $Au_{39}(SAd)_{23}$, $Au_{65}(SCy)_{30}$, and $Au_{67}(SCy)_{30}$. No $Au_{25}(SAd)_{18}$ was observed, which suggests that this structure would be too sterically crowded. Use of BLs may also lead to the discovery of new discrete sizes in other systems.

KEYWORDS: steric effects · bulky ligands · magic sizes · discrete sizes · clusters · gold · thiol

Ligand-stabilized nanoparticles (NPs) consist of crystalline, inorganic cores, coated with an organic shell. The combined novel physics of nanosized cores and the chemistry of the organic ligands present many opportunities for using the ligands to control NP properties, delivery, or assembly for many applications, including electronics, catalysis, medicine, and environmental remediation. An important issue in the synthesis of ligand-stabilized NPs is how the chemical properties of the ligand alter the size and chemical reactivity of the NP cores. In addition to other chemical effects (*e.g.*, bonding, charge, and polarity), the bulkiness of the ligand is expected to alter the reactivity of ligands during NP synthesis and affects the ability of the ligands to pack around the NP core. Here, we report a comprehensive study of the effects of bulky thiols on the synthesis of Au NPs, which results in smaller average NP sizes with a narrower size distribution and alters the discrete sizes to give fewer ligands per core atom. The term, discrete sizes, refers to small, stable NPs with molecular formulas, $M_m(L)_n$ (M = core atom, L = ligand), where certain pairs of integers *m* and *n* impart stability arising from geometrical and possibly electronic effects. Many mathematically plausible molecular formulas give clusters that lack stability and will usually decompose into molecular precursors or may be incorporated into larger NPs. For certain kinds of ligands, libraries of molecules with vastly differing bulkiness are commercially available, which include primary, secondary, and tertiary thiols, amines, and carboxylic acids. For phosphines, however, only tertiary structures are typically employed as ligands for NPs.

How steric effects in tertiary phosphines determine their chemistry in binding to metal ions and small metal clusters (typically containing fewer than 20 metal atoms) is well-known.[1−4] Bulkier groups on the phosphines generally decrease the cluster core size.[3,4] However, by controlling the reaction conditions, bulky groups on

* Address correspondence to jbtracy@ncsu.edu.

Received for review January 26, 2012 and accepted May 25, 2012.

Published online June 15, 2012
10.1021/nn3003778

phosphines can enable the synthesis of larger clusters, such as Schmid's Au_{55} and Rh_{55} clusters.[5−7] Murray and coworkers have reported evidence that use of bulky thiols in the synthesis of Au NPs alters the core size, but their investigations were chiefly concerned with other issues. Their results do not allow for a simple conclusion about the effects of bulky ligands. In comparison with linear alkanethiols, use of poly(ethylene glycol) thiol or tiopronin causes a reduction in the Au core diameter,[8,9] but phenyl-terminated thiols result in larger sizes.[10] Another study utilizing water-soluble thiols showed that different thiols gave different NP size distributions but did not significantly affect the average size.[11] In addition to ligand bulkiness, many reaction conditions (*e.g.*, concentrations, reducing agent, manner of addition and mixing, and temperature) also strongly affect the NP size, which limits the conclusions that can be drawn from comparing studies or reactions within the same study, where any of the other reaction conditions differed. There have also been several studies of how use of large, dendrimeric ligands affects the growth of metal NPs, which include comparisons of different dendrimer generations.[12−17] Some of these studies report decreased NP core sizes as the generation increases,[15−17] while others report increased core sizes.[12,14] The steric sizes of dendrimeric ligands are much larger than simple alkyl or aryl groups. Moreover, the branch points in dendrimeric ligands are several carbons removed from the α-carbon adjacent to the NP core, whereas the branch points in primary, secondary, and tertiary functional groups occur as close to the NP core as possible.

The aim of this study is to show significant effects that can only be attributed to differences in the bulkiness of the ligands (rather than to other chemical features of the ligands or to other variations in the reaction conditions). We show that use of bulky thiols in the synthesis of Au NPs results in smaller core sizes, sharpens the size distribution, and alters the discrete sizes. The finding of altered discrete sizes introduces important questions about their structure and stability.

Thiolate-stabilized Au NPs have been thoroughly studied[18] because of their novel structures,[19−23] electrochemical and optical properties,[24−26] and well-established surface chemistry[27−30] that bears some similarity to Au-thiolate self-assembled monolayers.[31] Thiolate-stabilized Au NPs can also serve as a model system for other kinds of ligand-stabilized NPs that are composed of air-sensitive core materials. The synthesis of Au-thiolate-stabilized NPs was first developed by Brust *et al.*,[32] in which successive addition of a thiol and $NaBH_4$ to Au(III) drives formation of Au NPs. This procedure can be performed with many different kinds of thiols, but it is known that chemical properties of the thiol can modify the thermodynamics and kinetics of NP growth. For example, thiophenols often exhibit behaviors different from aliphatic thiols[33−35] that could arise from differences in their electronic properties and steric sizes. In the formation of mixed-ligand monolayers, the monolayer composition can differ from the mole ratio of the precursors, which implies different chemical behaviors that depend on the nature of the ligand side chain.[36]

Bulky ligands (BLs) are routinely employed for synthesizing many kinds of NPs, which suggests that steric effects are important and often beneficial: Two common BLs are trioctylphosphine (TOP) and trioctylphosphine oxide (TOPO), which have been routinely used in the synthesis of semiconductor quantum dots[37,38] and Co[39−44] and Ni[45−47] NPs. Other bulky phosphines have been used for stabilizing small Ag, Cu, Cd, Hg, and Zn chalcogenide NPs.[48−52] Selected bulky thiols have been used for synthesizing metal NPs, such as functionalized[19,53−55] or unfunctionalized thiophenols[33−35] and amino acid derivatives (glutathione[11,56,57] and tiopronin[9,27]). In a few studies, some combinations of adamantane carboxylic acid, adamantane acetic acid, and adamantylamine have been used to synthesize highly monodisperse, small $CoPt_3$[58] and anisotropic, star- or flower-shaped magnetite[59] and PtRu[60] NPs.

This project was motivated by recent reports from Weiss and coworkers on the formation and chemistry of admantanethiolate (−SAd) self-assembled monolayers (SAMs) on Au surfaces.[61−66] Four main characteristics distinguish the novel properties of NPs stabilized by BLs (BL-NPs) from those of many conventional NPs stabilized by non-BLs (non-BL-NPs): (1) The steric hindrance of BLs is much greater than for non-BLs. BL-NPs are predicted to typically have smaller sizes than non-BLs because steric overlap for BLs increases as the NP size (radius of curvature) increases. In principle, growth of BL-NPs should terminate at small sizes because the large steric size of incoming BLs transporting inorganic precursors to the NP core during growth should prevent these incoming BLs from penetrating through the BL monolayer already covering the NP (Scheme 1). (2) The numerical density of ligands in the monolayer is lower for BLs than for non-BLs, corresponding to the differences in steric size.[61,67,68] For some small NPs, the ligand density is determined primarily by electronic stabilization (number of ligand head groups) rather than by the steric size.[69] In contrast, for BL-NPs, steric effects become significant.[70] (3) The interligand interactions in BL monolayers are weaker than for non-BL monolayers.[62] (4) The interstitial spaces in BL monolayers are larger than in non-BL monolayers,[71] which may facilitate the displacement of BLs by non-BLs.

We have chosen 1-adamantanethiol (AdSH), cyclohexanethiol (CySH), and *n*-hexanethiol (C6SH) as representative tertiary, secondary, and primary thiols, respectively. Aliphatic thiols were selected in order to isolate steric effects by minimizing chemical differences in the Au−S bond that would become more significant if aromatic thiols were used. Indeed, use of

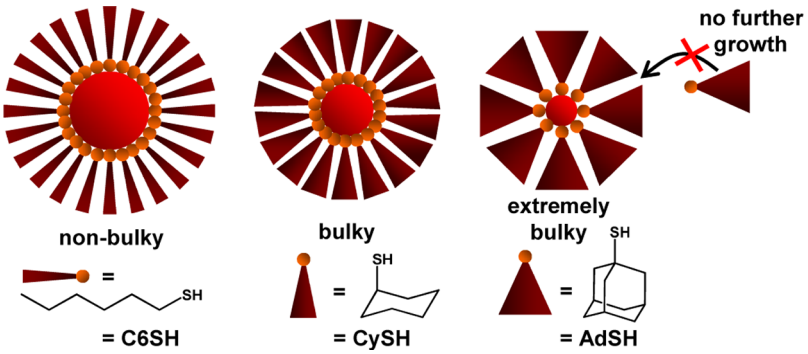

Scheme 1. Graphical depiction of the effects of bulky ligands (BLs) on nanoparticle size.

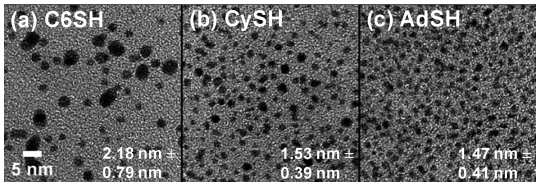

Figure 1. TEM images of Au nanoparticles synthesized using (a) *n*-hexanethiol (C6SH), (b) cyclohexanethiol (CySH), and (c) 1-adamantanethiol (AdSH).

BLs in the synthesis of Au NPs results in smaller core sizes, sharpens the size distribution, and alters the discrete sizes. Batches of Au NPs were synthesized using equimolar amounts of AdSH, CySH, or C6SH. Analysis by transmission electron microscopy (TEM) reveals that BLs provide smaller, more monodisperse sizes. As the bulkiness increases, the near-infrared luminescence increases, which is characteristic of the smallest Au NPs.[72,73] Four new discrete sizes were measured by MALDI-TOF mass spectrometry, $Au_{30}(SAd)_{18}$, $Au_{39}(SAd)_{23}$, $Au_{65}(SCy)_{30}$, and $Au_{67}(SCy)_{30}$. No $Au_{25}(SAd)_{18}$ was observed, which suggests that this structure would be too sterically crowded.

RESULTS AND DISCUSSION

Effects of Bulky Ligands. Size measurements by TEM (Figure 1) reveal larger average diameters and relative standard deviations (in parentheses) for the C6S-stabilized NPs of 2.18 nm (0.36), compared with 1.53 nm (0.26) and 1.47 nm (0.28) for the CyS- and AdS-stabilized NPs, respectively. Histograms of the diameter measurements are presented in the Supporting Information, Figure S1. Both the average size and relative standard deviation are smaller for the bulky CyS- and AdS-stabilized NPs than for C6S-stabilized NPs, which is consistent with the proposed mechanism for termination of growth when the radius of curvature increases such that additional BLs cannot be accommodated. This mechanism assumes that a high density of Au−S bonds is favorable, which would tend to sterically block delivery of Au to the core. If a high density of Au−S bonds was not favored, then more sparse coverage of the bulky thiolates might compensate

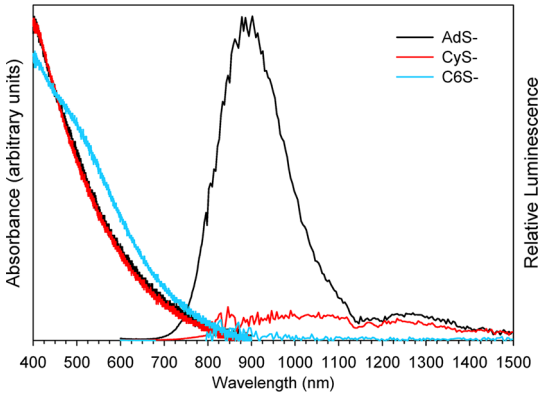

Figure 2. Absorbance and photoluminescence spectra (450 nm excitation) acquired in toluene. The small dip in the luminescence near 1150 nm arises from absorption caused by the third overtone of the C−H stretching vibration. The luminescence intensities were normalized to the absorbance at 450 nm.

for the large steric size, thus allowing the NPs to continue growing. Given that growth terminates at small sizes, we conclude that a high density of Au−S bonds is indeed favored. According to the TEM measurements, the sizes and size distributions of CyS- and AdS-stabilized NPs are quite similar, which implies that the core size may be reduced in more of a stepwise rather than continuous manner as the ligand bulkiness increases. Mass spectrometry measurements, however, show that stabilization by −SCy gives larger discrete sizes than −SAd.

Measurements of the optical absorbance (Figure 2) are consistent with the TEM size analysis. The C6S-stabilized NPs show the emergence of a weak surface plasmon resonance absorbance band, and the absorbance spectra for −SCy and −SAd stabilization are featureless and nearly identical. The CyS- and AdS-stabilized samples luminesce in the near-infrared (NIR) spectrum (Figure 2), and the luminescence intensity correlates with the steric size of the ligand: −SC6 < −SCy < −SAd. Such NIR luminescence is characteristic of the smallest thiolate-stabilized Au NPs (generally consisting of fewer than ~100 Au atoms), and the luminescence intensity generally increases as the size decreases.[73] Therefore, the AdS-stabilized sample appears to be

TABLE 1. Assignments of Parent and Fragment Ions

experimental mass (Da)	assignment	theoretical mass (Da)	$n^* = n - m$
11536[a]	**a** = $Au_{39}(SAd)_{23}$	11529	16
11400[a]	**a′** = $Au_{39}(SAd)_{22}(S)$	11394	
9891[a]	**a″** = $Au_{35}(SAd)_{18}$	9905	
8913[a]	**b** = $Au_{30}(SAd)_{18}$	8920	12
8777[a]	**b′** = $Au_{30}(SAd)_{17}(S)$	8785	
16652[b]	**c** = $Au_{67}(SCy)_{30}$	16653	37
16572[b]	**c′** = $Au_{67}(SCy)_{29}(S)$	16570	
16263[b]	**d** = $Au_{65}(SCy)_{30}$	16259	35
16183[b]	**d′** = $Au_{65}(SCy)_{29}(S)$	16176	

[a] Measured at 53% laser fluence. [b] Measured at 50% laser fluence.

particularly enriched in smaller NPs, even though TEM shows a similar size to the CyS-stabilized sample. Diameter measurements by TEM of ~1.5 nm are consistent with NPs consisting of roughly 100 Au atoms.[70] Such large Au NPs generally have rather weak luminescence,[73] and the stronger luminescence for the AdS-stabilized NPs is suspected to arise from smaller sizes. Accurately measuring the sizes of such small NPs by conventional TEM is challenging, and mass spectrometry (MS) was performed to search for discrete sizes and to assign precise molecular formulas. TEM, MS, and luminescence spectroscopy are highly complementary techniques because they are sensitive to different parts of the sample. Larger sizes are easier to image and measure with TEM, but MS measures the smallest NPs that also luminesce most intensely.

Assignments of Discrete Sizes. MS is ideally suited for assigning the molecular formulas of discrete sizes,[74−76] which are summarized in Table 1. MALDI-TOF-MS measurements were performed using the DCTB matrix, which is known to minimize fragmentation.[36] Systematic variation of the laser pulse intensity in positive linear mode gave spectra showing different regimes of behavior, including threshold ionization and fragmentation. The ion counts increased with the ligand bulkiness (−SC6 < −SCy < −SAd), which is fully consistent with the luminescence spectra and suggests increased content of discrete sizes with increasing bulkiness. Discrete sizes were identified for AdS- and CyS-stabilized NPs (Figure 3 and Supporting Information, Figures S2 and S3), but no discrete sizes were identified for C6S-stabilized NPs (Supporting Information, Figure S4). The parent ions were identified at the threshold laser fluence (46% for −SAd and 50% for −SCy). As the laser power was increased, substantial fragmentation occurred, thus depleting the parent ions and increasing the counts for the fragment ions. For AdS-stabilized NPs, we have identified two distinct parent ions with masses (measured at 53% fluence) of ~11 536 and ~8913 Da, which are assigned as **a** = $Au_{39}(SAd)_{23}$ and **b** = $Au_{30}(SAd)_{18}$. Three fragments, with masses of ~11 400, ~9891, and ~8777 Da, are assigned as **a′** = $Au_{39}(SAd)_{22}(S)$, **a″** = $Au_{35}(SAd)_{18}$, and **b′** = $Au_{30}(SAd)_{17}(S)$. For CyS-stabilized NPs, two parent

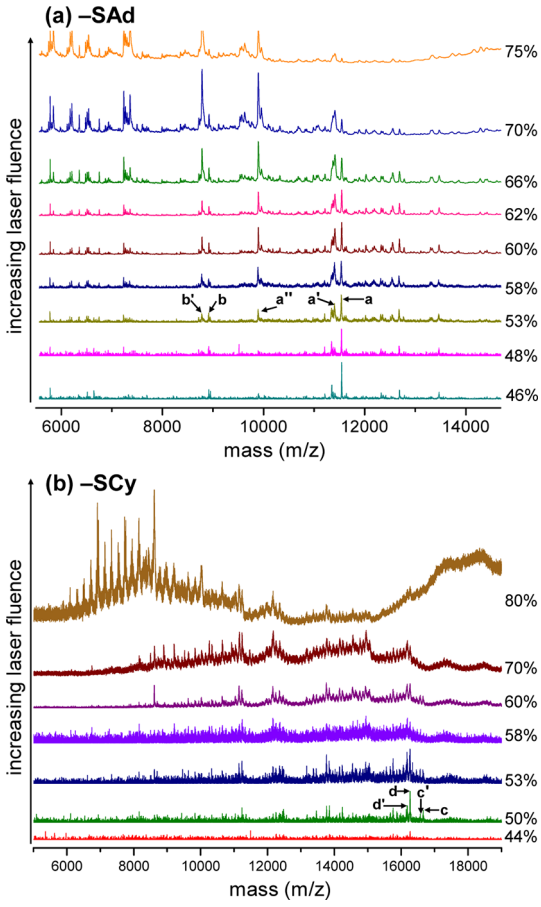

Figure 3. Positive-mode mass spectra of (a) AdS- and (b) CyS-stabilized Au nanoparticles using DCTB as the matrix for different laser powers. For −SAd, the counts for 46−58% were scaled by between 4 and 52×. For −SCy, the counts for 44−58% were scaled by 10×. Peaks a, b, c, and d indicate parent ions, and primed labels are for fragments.

ions with masses (measured at 50% fluence) of ~16 652 and ~16 263 Da were assigned as **c** = $Au_{67}(SCy)_{30}$ and **d** = $Au_{65}(SCy)_{30}$. Fragments were assigned as **c′** = $Au_{67}(SCy)_{29}(S)$ and **d′** = $Au_{65}(SCy)_{29}(S)$. Assignments are given only for peaks that can be clearly distinguished as parent or fragment ions. Some of the peaks at lower masses may also be parent ions, but we cannot confidently distinguish these peaks as parents rather than fragments.

Rationale for Assignments. Given limitations in the mass resolution and high-mass calibration, we have deduced no more than four possible assignments for each peak, of which only one is physically reasonable and consistent with assignments for related, discrete thiolate-stabilized Au NPs. Possible assignments for the parent ions were generated by first assuming singly charged ions (a standard assumption when analyzing MALDI-MS data of NPs). The NP composition was assumed to be $Au_n(SR)_m$, where m was varied between extremes of low to high ligand coverage and decimal values of n were calculated from the remainder of the mass not assigned to the ligands. Values of m and n are recorded in the Supporting Information, Tables S1 and

S2. For each value of m, if n was not near to an integer, no assignment was deemed possible. If n was within ± 0.05 of an integer, then such an assignment was deemed to be possible, though not necessarily physically reasonable. This threshold of ± 0.05 corresponds to an error of 10 Da, which is reasonable given the TOF detection and the high masses. It should be noted that repeating the analysis with data acquired at other laser intensities gives the same assignments.

In every case, only one of the possible assignments was physically reasonable. Only assignments having more Au atoms per ligand than non-BLs were considered due to the bulkiness of the −SAd and −SCy groups. For AdS-stabilized NPs, two mathematically possible assignments were determined for the peak at ~8913 Da, **b** = $Au_{30}(SAd)_{18}$ and $Au_{24}(SAd)_{25}$, but the latter is physically implausible. Two possible assignments were also derived for the peak at ~11 536 Da, $Au_{45}(SAd)_{16}$ and **a** = $Au_{39}(SAd)_{23}$. The first assignment is quite unlikely because it has a large number of additional Au atoms per ligand and significantly deviates from known trends for thiolate-stabilized Au NPs. Moreover, there is little reason to expect this heavier ion to have fewer ligands and many more Au atoms than **b**. Assignments **a** and **b** are consistent with general trends in ligand coverage for discrete-sized, thiolate-stabilized NPs, yet they show a modest enrichment in Au atoms per ligand, as predicted from the large steric size of the adamantyl group.

For the CyS-stabilized NPs, the difference in mass between the peaks at ~16 263 and ~16 652 Da is 389 Da, which can only correspond to two Au atoms. No combination of −SCy and Au atoms is close to 389 Da. For the peak at ~16 263 Da, three assignments may be initially considered, $Au_{72}(SCy)_{18}$, **d** = $Au_{65}(SCy)_{30}$, and $Au_{58}(SCy)_{42}$. $Au_{72}(SCy)_{18}$ is rather implausible, especially in consideration of **b** = $Au_{30}(SAd)_{18}$, which has the same number of bulkier ligands but many fewer Au atoms. $Au_{58}(SCy)_{42}$ is also unlikely since $Au_{68}(SCH_2CH_2Ph)_{34}$[77] is known, and $-SCH_2CH_2Ph$ is less bulky than −SCy. Therefore, **c** = $Au_{67}(SCy)_{30}$, based on the assignment of **d**.

Significance of New Discrete Sizes. Species **a**, **b**, **c**, and **d** are new discrete sizes that have more Au atoms per thiolate than previously known discrete sizes. These assignments are consistent with the expectation that fewer BLs rather than non-BLs could fit around a given number of core atoms. For comparison with **b** = $Au_{30}(SAd)_{18}$, we note that $Au_{25}(SR)_{18}$ is a common discrete size.[21,22,75] $Au_{29}(SR)_{20}$ has also been reported.[57] Similarly, for comparison with **a** = $Au_{39}(SAd)_{23}$, we note that $Au_{36}(SR)_{23}$,[35] $Au_{38}(SR)_{24}$,[23,78−81] $Au_{39}(SR)_{24}$,[57] and $Au_{40}(SR)_{24}$[82] have been reported. For comparison with **c** = $Au_{67}(SCy)_{30}$ and **d** = $Au_{65}(SCy)_{30}$, $Au_{55}(SR)_{31}$[83] and $Au_{68}(SR)_{34}$[77] are known. Several of these reports utilized somewhat bulky thiols, such as glutathione, phenylethanethiol, and thiophenol, but none of these are as bulky as AdSH. Notably, $Au_{36}(SR)_{23}$ was reported from use of thiophenol, but the effect might possibly be attributed to differences in thiolate bonding for aromatic and aliphatic thiolates.[35] Aliphatic thiols were selected for this study in order to separate the effects of bulkiness from aromaticity.

Discrete sizes can be stabilized by both geometrical and electronic stabilization. For assessing the electronic stabilization of a thiolate-stabilized, discrete-sized Au NP ion, $Au_n(SR)_m^{x+}$, the outermost electron shell contains $n^* = n - m - x$ electrons. Electronic stabilization is conferred for electron shell closings when n^* = 2, 8, 18, 34, 58,...[84] Values of n^* for the parent ions as neutrally charged species are given in Table 1. Closed electron shells might be achieved if the NPs exist as appropriately charged species, such as **a** as a dianion or **d** as a monocation, but **a**, **b**, **c**, and **d** otherwise have open electron shells. Here, we use the term "discrete" rather than "magic" sizes because magic sizes correspond to species with closed electron shells. Such nonmagic, discrete sizes nevertheless have sufficient thermodynamic or kinetic stability to provide for the existence of a relatively small number of highly abundant sizes rather than a broad distribution, where certain sizes would not be strongly favored over others. The relative importance of geometric and electronic stabilization for discrete-sized, thiolate-stabilized Au NPs in general has yet to be fully clarified. For example, $Au_{25}(SR)_{18}^-$ is a magic size ($n^* = 8$), but other oxidation states (0, +1, and +2) have been observed that do not have closed electron shells.[69,76,85] We further note that $Au_{38}(SR)_{24}$[23,78−81] is a commonly observed, nonmagic size ($n^* = 14$).

Remarkably, $Au_{25}(SAd)_{18}$ (7935 Da) and $Au_{25}(SCy)_{18}$ (6998 Da) do not appear in the mass spectra, which suggests that these structures would be too sterically crowded. Therefore, use of BLs can completely alter the discrete sizes by introducing new discrete sizes and destabilizing a well-known magic size. It is important to note, however, that $Au_{25}(SC6)_{18}$ is well-known[85−89] but was not observed in the mass spectra, likely because the reaction conditions favored larger sizes. For this reason, the existence of $Au_{25}(SCy)_{18}$ cannot be ruled out; another set of reaction conditions might favor smaller sizes, potentially including $Au_{25}(SCy)_{18}$.

Fragmentation. Loss of adamantyl and cyclohexyl groups appears to be the mechanism of fragmentation for **a**′, **b**′, **c**′, and **d**′. Scission of S−C bonds has previously been observed as a mode of fragmentation of thiolate-stabilized NPs in MALDI-MS.[36] Fragment **a**″ results from loss of $Au_4(SAd)_5$ from **a**. Loss of $Au_4(SR)_4$[90] is a common mode of fragmentation of thiolate-stabilized Au NPs.[36,74,91,92] Loss of an additional −SAd might be related to its large steric size. An alternative possible assignment for **a**″ is $Au_{34}(SAd)_{19}(S)$, which differs from $Au_{35}(SAd)_{18}$ by 2 Da and would arise

from loss of $Au_5(SAd)_3(Ad)$, but this alternate assignment is less probable because the fragment does not include a complete $Au_4(SAd)_4$ unit.

Structures of the Discrete Sizes. Comparison with the known structures of Au NPs stabilized by nonbulky thiolates and SAMs composed of bulky thiolates gives insight into the structural changes that may be anticipated in BL-NPs. For example, the surface density of thiolate bonds in −SAd SAMs on Au{111} surfaces is reduced to about 55% of that of linear alkanethiolates.[61,93] The surfaces of small Au NPs stabilized by nonbulky thiolates are covered by linear −SR−Au−SR− or −SR−Au−SR−Au−SR− chains[19−23] anchored to the Au core at both ends, which are called "staples". The absence of $Au_{25}(SAd)_{18}$ indicates that the $Au_{25}(SR-)_{18}$ structure[21,22] would be too compact for −SAd ligands. Steric overlap between ligands within different staples might force greater spacing between the staples. Steric overlap could also occur within the same staple, resulting in a strained conformation, thereby modifying (most likely, increasing) the distance between the anchor points to the core. Alternatively, steric overlap between neighboring −SAd ligands might be severe enough to prevent the formation of staples; a recent study of −SAd SAMs on Au{111} showed that −SAd binds to only one surface Au adatom, whereas nonbulky thiolates bind to two adatoms.[93] Each of these possibilities would expand the volume of the Au core. It should be noted that **b** accommodates five more Au atoms than $Au_{25}(SR)_{18}$, while having the same number of thiolates, though it remains unclear how closely the structures are related.

Further studies are needed to predict and understand the structures of BL-NPs. Many cage molecules[66] are available for investigating how the steric size or shape alters the discrete sizes,[65] and use of 2-adamantanethiol could reveal how the orientation of the adamantyl groups affects the NP structure. An additional study could also investigate the use of mixtures of BLs and non-BLs in the NP synthesis. Since non-BLs are less sterically demanding, could use of even a small amount of non-BLs relax steric strain and make the discrete sizes for non-BLs favorable?

CONCLUSIONS

In summary, the use of BLs in the synthesis of thiolate-stabilized NPs results in smaller sizes and improves the monodispersity, but perfect monodispersity is not achieved. Optimization of the reaction conditions for each ligand may further improve the monodispersity. Use of AdSH yields a mixture of discrete-sized NPs, from which two predominant sizes, $Au_{30}(SAd)_{18}$ and $Au_{39}(SAd)_{23}$, have been identified by MALDI-TOF-MS. Two larger discrete sizes, $Au_{65}(SCy)_{30}$ and $Au_{67}(SCy)_{30}$, have been obtained using CySH. As a consequence of the large size of the −SAd and −SCy moieties, these discrete sizes have more Au atoms per thiolate than previously known discrete-sized Au NPs that utilized less bulky ligands. No $Au_{25}(SAd)_{18}$ was observed in the mass spectra, which underscores the ability of BLs to stabilize new discrete sizes and to destabilize a well-known magic size for less bulky ligands. Use of BLs in other systems may also lead to the discovery of new discrete sizes.

An assumption implicit in the mechanism of size reduction using bulky thiolates is that a high density of ligand coverage and thus of Au−S bonds is favorable, which exacerbates the steric overlap of BLs. In addition to the standard geometrical and electronic effects that must be considered for all kinds of discrete-sized NPs, the energetic balance between high ligand density and steric overlap has an important role in determining the molecular formulas and structures of discrete-sized NPs stabilized by BLs. There is a great need for theoretical studies of BL-NPs that will give additional insight into how the optimal size and ligand coverage for BL-NPs are determined.

EXPERIMENTAL SECTION

Nanoparticle Synthesis. A solution of 288 mg (0.731 mmol) of $HAuCl_4 \cdot 3H_2O$ (99.99%, Alfa Aesar) in 9.0 mL of distilled water was vigorously mixed with a solution of 468 mg (0.856 mmol) of tetraoctylammonium bromide (Oct_4NBr, 98%, Acros) in 18.0 mL of toluene. The mixture was stirred for 30 min at room temperature, during which the aqueous phase changed from yellow to colorless, and the toluene phase became colored red. After removing the aqueous phase, the toluene mixture was fractionated into 6.0 mL aliquots that were transferred into three flasks. One of the following thiols was added to each flask in a 10:1 thiol/Au molar ratio: 1-adamantanethiol (AdSH, 95%, Sigma-Aldrich), cyclohexanethiol (CySH, 99%, Alfa Aesar), or *n*-hexanethiol (C6SH, 97%, Alfa Aesar). Each mixture was stirred for 30−60 min, during which the solution became colorless, and then each flask was cooled to 0 °C in an ice bath. A solution of 390 mg (10.3 mmol) of $NaBH_4$ (98%, J.T. Baker) was prepared in 0.9 mL of distilled water at 0 °C. The $NaBH_4$ solution was loaded into three syringes in amounts of 0.3 mL each, and one syringe was quickly injected into each reaction flask while stirring vigorously. Each solution became dark brown or black in color and was stirred for 1 h at 0 °C.

Purification. Upon completing each reaction, the toluene was separated from the aqueous layer. An excess of methanol was added to each toluene solution to flocculate the NPs. In some instances, flocculation was incomplete; concentrating the NP solution using a rotary evaporator before adding the methanol ensured complete flocculation. The NPs were repeatedly (4−5 times) isolated by centrifugation, resuspended in a small amount of toluene, and flocculated again. The final product was stored as a solid in the dark after removing the toluene using a rotary evaporator. Specimens for TEM were prepared by allowing a drop of the NP solution placed on an ultrathin, amorphous carbon and Formvar substrate to evaporate.

Transmission Electron Microscopy (TEM). Bright-field TEM images were acquired using a JEOL 2000FX microscope. The average NP diameters were obtained from measurements of 100 NPs from each sample using publicly available ImageJ software.[94]

Absorbance and Luminescence Spectroscopy. Dilute solutions of NPs in toluene were measured in a quartz optical cell. Optical absorbance spectra were acquired using an Ocean Optics CHEMUSB4-VIS-NIR spectrophotometer. The concentrations were adjusted such that the absorbance at the excitation wavelength (450 nm) would be near 0.1. Emission spectra were acquired using a Photon Technology International Inc., QuantaMaster 4SE-NIR5 spectrometer equipped with Hamamatsu R928P PMT and InGaAs detectors for the visible and near-infrared (NIR) regions of the spectrum, respectively. The emission spectra were corrected for the spectral response of each detector. All excitation and emission slits were set to 2.5 mm. A 550−2000 nm band-pass filter was placed before the PMT detector, and a 760 nm long-pass filter was placed before the InGaAs detector. The luminescence spectra were normalized to the absorbance at 450 nm, and the spectra from the PMT and InGaAs detectors were manually joined together between 798 and 802 nm.

Matrix-Assisted Laser Desorption Ionization Time-of-Flight Mass Spectrometry (MALDI-TOF-MS). Solutions of the 100 mM *trans*-2-[3-(4-*tert*-butylphenyl)-2-methyl-2-propenylidene]malononitrile (DCTB) matrix[36] and analyte (7.4 mg/mL) were prepared in toluene and were mixed in microcentrifuge tubes at a 100:1 matrix/analyte volume ratio. For each sample, 1 μL of this solution was applied to the sample plate and allowed to dry under ambient atmosphere. Positive-mode mass spectra were acquired using a Shimadzu AXIMA Assurance laser desorption linear time-of-flight (MALDI-TOF) mass spectrometer equipped with a nitrogen laser (337 nm). The accelerating voltage was held at 19.9 kV. For AdS-stabilized NPs, standards of bovine insulin (5734 Da), human insulin (5808 Da), and cytochrome *c* (12 362 Da) were used for a three-point calibration. For CyS-stabilized NPs, standards of insulin B (3494 Da), cytochrome *c* (12 362 Da), and apomyoglobin (16 952 Da) were used for a three-point calibration. The mass spectra presented in Figure 3 and Supporting Information Figure S4 were not smoothed, and the expanded mass spectra in the Supporting Information, Figures S2 and S3, were smoothed using boxcar averaging with a width of 10 data points.

Conflict of Interest: The authors declare no competing financial interest.

Acknowledgment. This work was supported by the National Science Foundation (CBET-0967559 and DMR-1056653) and startup funds from North Carolina State University. A.C.J.-P. acknowledges support from a GAANN fellowship. We thank K. Brennaman and T. Meyer for assistance with the emission spectroscopy measurements, D. Muddiman for helpful discussions and assistance with mass spectrometry measurements, and C. Aikens for helpful discussions. The Molecular Weight Calculator is supported by the Department of Energy.

Supporting Information Available: Histograms of TEM size measurements, mass spectrum for C6S-stabilized NPs, expanded mass spectra, and tables of possible assignments of discrete sizes. This material is available free of charge *via* the Internet at http://pubs.acs.org.

REFERENCES AND NOTES

1. Tolman, C. A. Steric Effects of Phosphorus Ligands in Organometallic Chemistry and Homogeneous Catalysis. *Chem. Rev.* **1977**, *77*, 313–348.
2. Mingos, D. M. P. Steric Effects in Metal Cluster Compounds. *Inorg. Chem.* **1982**, *21*, 464–466.
3. Hall, K. P.; Mingos, D. M. P. Homonuclear and Heteronuclear Cluster Compounds of Gold. *Prog. Inorg. Chem.* **1984**, *32*, 237–325.
4. Mingos, D. M. P.; Wales, D. J. *Introduction to Cluster Chemistry*; Prentice Hall: Englewood Cliffs, NJ, 1990.
5. Schmid, G.; Pfeil, R.; Boese, R.; Bandermann, F.; Meyer, S.; Calis, G. H. M.; van der Velden, J. W. A. $Au_{55}[P(C_6H_5)_3]_{12}Cl_6$ - Ein Goldcluster Ungewöhnlicher Größe. *Chem. Ber.* **1981**, *114*, 3634–3642.
6. Schmid, G.; Giebel, U.; Huster, W.; Schwenk, A. Large Transition Metal Clusters, 2. Synthesis and Properties of $Rh_{55}[P(tert\text{-}Bu)_3]_{12}Cl_{20}$. *Inorg. Chim. Acta* **1984**, *85*, 97–102.
7. Schmid, G. *Developments in Transition Metal Cluster Chemistry - The Way to Large Clusters*; Springer: Berlin, 1985; Vol. 62, pp 51−85.
8. Wuelfing, W. P.; Gross, S. M.; Miles, D. T.; Murray, R. W. Nanometer Gold Clusters Protected by Surface-Bound Monolayers of Thiolated Poly(ethylene glycol) Polymer Electrolyte. *J. Am. Chem. Soc.* **1998**, *120*, 12696–12697.
9. Templeton, A. C.; Chen, S.; Gross, S. M.; Murray, R. W. Water-Soluble, Isolable Gold Clusters Protected by Tiopronin and Coenzyme A Monolayers. *Langmuir* **1999**, *15*, 66–76.
10. Chen, S.; Murray, R. W. Arenethiolate Monolayer-Protected Gold Clusters. *Langmuir* **1999**, *15*, 682–689.
11. Negishi, Y.; Takasugi, Y.; Sato, S.; Yao, H.; Kimura, K.; Tsukuda, T. Kinetic Stabilization of Growing Gold Clusters by Passivation with Thiolates. *J. Phys. Chem. B* **2006**, *110*, 12218–12221.
12. Wang, R.; Yang, J.; Zheng, Z.; Carducci, M. D.; Jiao, J.; Seraphin, S. Dendron-Controlled Nucleation and Growth of Gold Nanoparticles. *Angew. Chem., Int. Ed.* **2001**, *40*, 549–552.
13. Kim, M.-K.; Jeon, Y.-M.; Jeon, W. S.; Kim, H.-J.; Hong, S. G.; Park, C. G.; Kim, K. Novel Dendron-Stabilized Gold Nanoparticles with High Stability and Narrow Size Distribution. *Chem. Commun.* **2001**, 667–668.
14. Nakao, S.; Torigoe, K.; Kon-No, K.; Yonezawa, T. Self-Assembled One-Dimensional Arrays of Gold−Dendron Nanocomposites. *J. Phys. Chem. B* **2002**, *106*, 12097–12100.
15. Love, C. S.; Chechik, V.; Smith, D. K.; Brennan, C. Dendron-Stabilised Gold Nanoparticles: Generation Dependence of Core Size and Thermal Stability. *J. Mater. Chem.* **2004**, *14*, 919–923.
16. Love, C. S.; Ashworth, I.; Brennan, C.; Chechik, V.; Smith, D. K. Dendron-Protected Au Nanoparticles - Effect of Dendritic Structure on Chemical Stability. *J. Colloid Interface Sci.* **2006**, *302*, 178–186.
17. Mizugaki, T.; Murata, M.; Fukubayashi, S.; Mitsudome, T.; Jitsukawa, K.; Kaneda, K. PAMAM Dendron-Stabilised Palladium Nanoparticles: Effect of Generation and Peripheral Groups on Particle Size and Hydrogenation Activity. *Chem. Commun.* **2008**, 241–243.
18. Daniel, M.-C.; Astruc, D. Gold Nanoparticles: Assembly, Supramolecular Chemistry, Quantum-Size-Related Properties, and Applications toward Biology, Catalysis, and Nanotechnology. *Chem. Rev.* **2004**, *104*, 293–346.
19. Jadzinsky, P. D.; Calero, G.; Ackerson, C. J.; Bushnell, D. A.; Kornberg, R. D. Structure of a Thiol Monolayer-Protected Gold Nanoparticle at 1.1 Angstrom Resolution. *Science* **2007**, *318*, 430–433.
20. Jiang, D. E.; Tiago, M. L.; Luo, W. D.; Dai, S. The "Staple" Motif: A Key to Stability of Thiolate-Protected Gold Nanoclusters. *J. Am. Chem. Soc.* **2008**, *130*, 2777–2779.
21. Heaven, M. W.; Dass, A.; White, P. S.; Holt, K. M.; Murray, R. W. Crystal Structure of the Gold Nanoparticle $[N(C_8H_{17})_4][Au_{25}(SCH_2CH_2Ph)_{18}]$. *J. Am. Chem. Soc.* **2008**, *130*, 3754–3755.
22. Zhu, M.; Aikens, C. M.; Hollander, F. J.; Schatz, G. C.; Jin, R. Correlating the Crystal Structure of a Thiol-Protected Au_{25} Cluster and Optical Properties. *J. Am. Chem. Soc.* **2008**, *130*, 5883–5885.
23. Qian, H. F.; Eckenhoff, W. T.; Zhu, Y.; Pintauer, T.; Jin, R. C. Total Structure Determination of Thiolate-Protected Au_{38} Nanoparticles. *J. Am. Chem. Soc.* **2010**, *132*, 8280–8281.
24. Murray, R. W. Nanoelectrochemistry: Metal Nanoparticles, Nanoelectrodes, and Nanopores. *Chem. Rev.* **2008**, *108*, 2688–2720.
25. Sardar, R.; Funston, A. M.; Mulvaney, P.; Murray, R. W. Gold Nanoparticles: Past, Present, and Future. *Langmuir* **2009**, *25*, 13840–13851.
26. Jin, R. C. Quantum Sized, Thiolate-Protected Gold Nanoclusters. *Nanoscale* **2010**, *2*, 343–362.
27. Hostetler, M. J.; Templeton, A. C.; Murray, R. W. Dynamics of Place-Exchange Reactions on Monolayer-Protected Gold Cluster Molecules. *Langmuir* **1999**, *15*, 3782–3789.

28. DeVries, G. A.; Brunnbauer, M.; Hu, Y.; Jackson, A. M.; Long, B.; Neltner, B. T.; Uzun, O.; Wunsch, B. H.; Stellacci, F. Divalent Metal Nanoparticles. *Science* **2007**, *315*, 358–361.
29. Jackson, A. M.; Myerson, J. W.; Stellacci, F. Spontaneous Assembly of Subnanometre-Ordered Domains in the Ligand Shell of Monolayer-Protected Nanoparticles. *Nat. Mater.* **2004**, *3*, 330–336.
30. Ionita, P.; Caragheorgheopol, A.; Gilbert, B. C.; Chechik, V. EPR Study of a Place-Exchange Reaction on Au Nanoparticles: Two Branches of a Disulfide Molecule Do Not Adsorb Adjacent to Each Other. *J. Am. Chem. Soc.* **2002**, *124*, 9048–9049.
31. Love, J. C.; Estroff, L. A.; Kriebel, J. K.; Nuzzo, R. G.; Whitesides, G. M. Self-Assembled Monolayers of Thiolates on Metals as a Form of Nanotechnology. *Chem. Rev.* **2005**, *105*, 1103–1169.
32. Brust, M.; Walker, M.; Bethell, D.; Schiffrin, D. J.; Whyman, R. Synthesis of Thiol-Derivatized Gold Nanoparticles in a Two-Phase Liquid–Liquid System. *J. Chem. Soc., Chem. Commun.* **1994**, 801–802.
33. Price, R. C.; Whetten, R. L. All-Aromatic, Nanometer-Scale, Gold-Cluster Thiolate Complexes. *J. Am. Chem. Soc.* **2005**, *127*, 13750–13751.
34. Price, R. C.; Whetten, R. L. Raman Spectroscopy of Benzenethiolates on Nanometer-Scale Gold Clusters. *J. Phys. Chem. B* **2006**, *110*, 22166–22171.
35. Nimmala, P. R.; Dass, A. $Au_{36}(SPh)_{23}$ Nanomolecules. *J. Am. Chem. Soc.* **2011**, *133*, 9175–9177.
36. Dass, A.; Stevenson, A.; Dubay, G. R.; Tracy, J. B.; Murray, R. W. Nanoparticle MALDI-TOF Mass Spectrometry without Fragmentation: $Au_{25}(SCH_2CH_2Ph)_{18}$ and Mixed Monolayer $Au_{25}(SCH_2CH_2Ph)_{18-x}L_x$. *J. Am. Chem. Soc.* **2008**, *130*, 5940–5946.
37. Murray, C. B.; Norris, D. J.; Bawendi, M. G. Synthesis and Characterization of Nearly Monodisperse CdE (E = S, Se, Te) Semiconductor Nanocrystallites. *J. Am. Chem. Soc.* **1993**, *115*, 8706–8715.
38. Peng, X. G.; Manna, L.; Yang, W. D.; Wickham, J.; Scher, E.; Kadavanich, A.; Alivisatos, A. P. Shape Control of CdSe Nanocrystals. *Nature* **2000**, *404*, 59–61.
39. Sun, S. H.; Murray, C. B. Synthesis of Monodisperse Cobalt Nanocrystals and Their Assembly into Magnetic Superlattices (Invited). *J. Appl. Phys.* **1999**, *85*, 4325–4330.
40. Puntes, V. F.; Krishnan, K. M.; Alivisatos, A. P. Colloidal Nanocrystal Shape and Size Control: The Case of Cobalt. *Science* **2001**, *291*, 2115–2117.
41. Puntes, V. F.; Zanchet, D.; Erdonmez, C. K.; Alivisatos, A. P. Synthesis of hcp-Co Nanodisks. *J. Am. Chem. Soc.* **2002**, *124*, 12874–12880.
42. Bao, Y. P.; Beerman, M.; Pakhomov, A. B.; Krishnan, K. M. Controlled Crystalline Structure and Surface Stability of Cobalt Nanocrystals. *J. Phys. Chem. B* **2005**, *109*, 7220–7222.
43. Tracy, J. B.; Weiss, D. N.; Dinega, D. P.; Bawendi, M. G. Exchange Biasing and Magnetic Properties of Partially and Fully Oxidized Colloidal Cobalt Nanoparticles. *Phys. Rev. B* **2005**, *72*, 064404.
44. Bao, Y. P.; Calderon, H.; Krishnan, K. M. Synthesis and Characterization of Magnetic-Optical Co–Au Core–Shell Nanoparticles. *J. Phys. Chem. C* **2007**, *111*, 1941–1944.
45. Lee, W. R.; Kim, M. G.; Choi, J. R.; Park, J. I.; Ko, S. J.; Oh, S. J.; Cheon, J. Redox-Transmetalation Process as a Generalized Synthetic Strategy for Core–Shell Magnetic Nanoparticles. *J. Am. Chem. Soc.* **2005**, *127*, 16090–16097.
46. Lee, I. S.; Lee, N.; Park, J.; Kim, B. H.; Yi, Y. W.; Kim, T.; Kim, T. K.; Lee, I. H.; Paik, S. R.; Hyeon, T. Ni/NiO Core/Shell Nanoparticles for Selective Binding and Magnetic Separation of Histidine-Tagged Proteins. *J. Am. Chem. Soc.* **2006**, *128*, 10658–10659.
47. Johnston-Peck, A. C.; Wang, J.; Tracy, J. B. Synthesis and Structural and Magnetic Characterization of Ni(Core)/NiO(Shell) Nanoparticles. *ACS Nano* **2009**, *3*, 1077–1084.
48. Müller, A.; Fenske, D.; Kögerler, P. From Giant Molecular Clusters and Precursors to Solid-State Structures. *Curr. Opin. Solid State Mater. Sci.* **1999**, *4*, 141–153.
49. Dehnen, S.; Eichhöfer, A.; Fenske, D. Chalcogen-Bridged Copper Clusters. *Eur. J. Inorg. Chem.* **2002**, 279–317.
50. Corrigan, J. F.; Fuhr, O.; Fenske, D. Metal Chalcogenide Clusters on the Border between Molecules and Materials. *Adv. Mater.* **2009**, *21*, 1867–1871.
51. Evans, C. M.; Evans, M. E.; Krauss, T. D. Mysteries of TOPSe Revealed: Insights into Quantum Dot Nucleation. *J. Am. Chem. Soc.* **2010**, *132*, 10973–10975.
52. Cossairt, B. M.; Owen, J. S. CdSe Clusters: At the Interface of Small Molecules and Quantum Dots. *Chem. Mater.* **2011**, *23*, 3114–3119.
53. Branham, M. R.; Douglas, A. D.; Mills, A. J.; Tracy, J. B.; White, P. S.; Murray, R. W. Arylthiolate-Protected Silver Quantum Dots. *Langmuir* **2006**, *22*, 11376–11383.
54. Bakr, O. M.; Amendola, V.; Aikens, C. M.; Wenseleers, W.; Lee, R.; Dal Negro, L.; Schatz, G. C.; Stellacci, F. Silver Nanoparticles with Broad Multi-Band Linear Optical Absorption. *Angew. Chem., Int. Ed.* **2009**, *48*, 5921–5926.
55. Negishi, Y.; Arai, R.; Niihori, Y.; Tsukuda, T. Isolation and Structural Characterization of Magic Silver Clusters Protected by 4-(*tert*-Butyl)benzyl Mercaptan. *Chem. Commun.* **2011**, *47*, 5693–5695.
56. Link, S.; Beeby, A.; Fitzgerald, S.; El-Sayed, M. A.; Schaaff, T. G.; Whetten, R. L. Visible to Infrared Luminescence from a 28-Atom Gold Cluster. *J. Phys. Chem. B* **2002**, *106*, 3410–3415.
57. Negishi, Y.; Nobusada, K.; Tsukuda, T. Glutathione-Protected Gold Clusters Revisited: Bridging the Gap between Gold(I)–Thiolate Complexes and Thiolate-Protected Gold Nanocrystals. *J. Am. Chem. Soc.* **2005**, *127*, 5261–5270.
58. Shevchenko, E. V.; Talapin, D. V.; Rogach, A. L.; Kornowski, A.; Haase, M.; Weller, H. Colloidal Synthesis and Self-Assembly of $CoPt_3$ Nanocrystals. *J. Am. Chem. Soc.* **2002**, *124*, 11480–11485.
59. Zhang, L.; Dou, Y. H.; Gu, H. C. Sterically Induced Shape Control of Magnetite Nanoparticles. *J. Cryst. Growth* **2006**, *296*, 221–226.
60. Teng, X. W.; Maksimuk, S.; Frommer, S.; Yang, H. Three-Dimensional PtRu Nanostructures. *Chem. Mater.* **2007**, *19*, 36–41.
61. Dameron, A. A.; Charles, L. F.; Weiss, P. S. Structures and Displacement of 1-Adamantanethiol Self-Assembled Monolayers on Au{111}. *J. Am. Chem. Soc.* **2005**, *127*, 8697–8704.
62. Dameron, A. A.; Mullen, T. J.; Hengstebeck, R. W.; Saavedra, H. M.; Weiss, P. S. Origins of Displacement in 1-Adamantanethiolate Self-Assembled Monolayers. *J. Phys. Chem. C* **2007**, *111*, 6747–6752.
63. Mullen, T. J.; Dameron, A. A.; Saavedra, H. M.; Williams, M. E.; Weiss, P. S. Dynamics of Solution Displacement in 1-Adamantanethiolate Self-Assembled Monolayers. *J. Phys. Chem. C* **2007**, *111*, 6740–6746.
64. Saavedra, H. M.; Barbu, C. M.; Dameron, A. A.; Mullen, T. J.; Crespi, V. H.; Weiss, P. S. 1-Adamantanethiolate Monolayer Displacement Kinetics Follow a Universal Form. *J. Am. Chem. Soc.* **2007**, *129*, 10741–10746.
65. Kim, M.; Hohman, J. N.; Morin, E. I.; Daniel, T. A.; Weiss, P. S. Self-Assembled Monolayers of 2-Adamantanethiol on Au{111}: Control of Structure and Displacement. *J. Phys. Chem. A* **2009**, *113*, 3895–3903.
66. Hohman, J. N.; Claridge, S. A.; Kim, M.; Weiss, P. S. Cage Molecules for Self-Assembly. *Mater. Sci. Eng., R* **2010**, *70*, 188–208.
67. Hill, H. D.; Millstone, J. E.; Banholzer, M. J.; Mirkin, C. A. The Role Radius of Curvature Plays in Thiolated Oligonucleotide Loading on Gold Nanoparticles. *ACS Nano* **2009**, *3*, 418–424.
68. Jiménez, A.; Sarsa, A.; Blázquez, M.; Pineda, T. A Molecular Dynamics Study of the Surfactant Surface Density of Alkanethiol Self-Assembled Monolayers on Gold Nanoparticles as a Function of the Radius. *J. Phys. Chem. C* **2010**, *114*, 21309–21314.
69. Tracy, J. B.; Crowe, M. C.; Parker, J. F.; Hampe, O.; Fields-Zinna, C. A.; Dass, A.; Murray, R. W. Electrospray Ionization Mass Spectrometry of Uniform and Mixed Monolayer

Nanoparticles: $Au_{25}[S(CH_2)_2Ph]_{18}$ and $Au_{25}[S(CH_2)_2Ph]_{18-x}(SR)_x$. *J. Am. Chem. Soc.* **2007**, *129*, 16209–16215.
70. Wolfe, R. L.; Balasubramanian, R.; Tracy, J. B.; Murray, R. W. Fully Ferrocenated Hexanethiolate Monolayer-Protected Gold Clusters. *Langmuir* **2007**, *23*, 2247–2254.
71. de Silva, N.; Ha, J.-M.; Solovyov, A.; Nigra, M. M.; Ogino, I.; Yeh, S. W.; Durkin, K. A.; Katz, A. A Bioinspired Approach for Controlling Accessibility in Calix[4]arene-Bound Metal Cluster Catalysts. *Nat. Chem.* **2010**, *2*, 1062–1068.
72. Bigioni, T. P.; Whetten, R. L.; Dag, Ö. Near-Infrared Luminescence from Small Gold Nanocrystals. *J. Phys. Chem. B* **2000**, *104*, 6983–6986.
73. Wang, G. L.; Huang, T.; Murray, R. W.; Menard, L.; Nuzzo, R. G. Near-IR Luminescence of Monolayer-Protected Metal Clusters. *J. Am. Chem. Soc.* **2005**, *127*, 812–813.
74. Harkness, K. M.; Cliffel, D. E.; McLean, J. A. Characterization of Thiolate-Protected Gold Nanoparticles by Mass Spectrometry. *Analyst* **2010**, *135*, 868–874.
75. Parker, J. F.; Fields-Zinna, C. A.; Murray, R. W. The Story of a Monodisperse Gold Nanoparticle: $Au_{25}L_{18}$. *Acc. Chem. Res.* **2010**, *43*, 1289–1296.
76. Dass, A. Nano-Scaling Law: Geometric Foundation of Thiolated Gold Nanomolecules. *Nanoscale* **2012**, *4*, 2260–2263.
77. Dass, A. Mass Spectrometric Identification of $Au_{68}(SR)_{34}$ Molecular Gold Nanoclusters with 34-Electron Shell Closing. *J. Am. Chem. Soc.* **2009**, *131*, 11666–11667.
78. Chaki, N. K.; Negishi, Y.; Tsunoyama, H.; Shichibu, Y.; Tsukuda, T. Ubiquitous 8 and 29 kDa Gold:Alkanethiolate Cluster Compounds: Mass-Spectrometric Determination of Molecular Formulas and Structural Implications. *J. Am. Chem. Soc.* **2008**, *130*, 8608–8610.
79. Qian, H. F.; Zhu, M. Z.; Lanni, E.; Zhu, Y.; Bier, M. E.; Jin, R. C. Conversion of Polydisperse Au Nanoparticles into Monodisperse Au_{25} Nanorods and Nanospheres. *J. Phys. Chem. C* **2009**, *113*, 17599–17603.
80. Qian, H. F.; Zhu, Y.; Jin, R. C. Size-Focusing Synthesis, Optical and Electrochemical Properties of Monodisperse $Au_{38}(SC_2H_4Ph)_{24}$ Nanoclusters. *ACS Nano* **2009**, *3*, 3795–3803.
81. Knoppe, S.; Dharmaratne, A. C.; Schreiner, E.; Dass, A.; Bürgi, T. Ligand Exchange Reactions on Au_{38} and Au_{40} Clusters: A Combined Circular Dichroism and Mass Spectrometry Study. *J. Am. Chem. Soc.* **2010**, *132*, 16783–16789.
82. Qian, H.; Zhu, Y.; Jin, R. Isolation of Ubiquitous $Au_{40}(SR)_{24}$ Clusters from the 8 kDa Gold Clusters. *J. Am. Chem. Soc.* **2010**, *132*, 4583–4585.
83. Qian, H.; Jin, R. Synthesis and Electrospray Mass Spectrometry Determination of Thiolate-Protected $Au_{55}(SR)_{31}$ Nanoclusters. *Chem. Commun.* **2011**, *47*, 11462–11464.
84. Walter, M.; Akola, J.; Lopez-Acevedo, O.; Jadzinsky, P. D.; Calero, G.; Ackerson, C. J.; Whetten, R. L.; Grönbeck, H.; Häkkinen, H. A Unified View of Ligand-Protected Gold Clusters as Superatom Complexes. *Proc. Natl. Acad. Sci. U. S.A.* **2008**, *105*, 9157–9162.
85. Negishi, Y.; Chaki, N. K.; Shichibu, Y.; Whetten, R. L.; Tsukuda, T. Origin of Magic Stability of Thiolated Gold Clusters: A Case Study on $Au_{25}(SC_6H_{13})_{18}$. *J. Am. Chem. Soc.* **2007**, *129*, 11322–11323.
86. Jimenez, V. L.; Georganopoulou, D. G.; White, R. J.; Harper, A. S.; Mills, A. J.; Lee, D.; Murray, R. W. Hexanethiolate Monolayer Protected 38 Gold Atom Cluster. *Langmuir* **2004**, *20*, 6864–6870.
87. Dass, A.; Holt, K.; Parker, J. F.; Feldberg, S. W.; Murray, R. W. Mass Spectrometrically Detected Statistical Aspects of Ligand Populations in Mixed Monolayer $Au_{25}L_{18}$ Nanoparticles. *J. Phys. Chem. C* **2008**, *112*, 20276–20283.
88. Parker, J. F.; Weaver, J. E. F.; McCallum, F.; Fields-Zinna, C. A.; Murray, R. W. Synthesis of Monodisperse $[Oct_4N^+][Au_{25}(SR)_{18}^-]$ Nanoparticles, with Some Mechanistic Observations. *Langmuir* **2010**, *26*, 13650–13654.
89. Kumar, S. S.; Kwak, K.; Lee, D. Electrochemical Sensing Using Quantum-Sized Gold Nanoparticles. *Anal. Chem.* **2011**, *83*, 3244–3247.
90. Grönbeck, H.; Walter, M.; Häkkinen, H. Theoretical Characterization of Cyclic Thiolated Gold Clusters. *J. Am. Chem. Soc.* **2006**, *128*, 10268–10275.
91. Gies, A. P.; Hercules, D. M.; Gerdon, A. E.; Cliffel, D. E. Electrospray Mass Spectrometry Study of Tiopronin Monolayer-Protected Gold Nanoclusters. *J. Am. Chem. Soc.* **2007**, *129*, 1095–1104.
92. Fields-Zinna, C. A.; Sampson, J. S.; Crowe, M. C.; Tracy, J. B.; Parker, J. F.; deNey, A. M.; Muddiman, D. C.; Murray, R. W. Tandem Mass Spectrometry of Thiolate-Protected Au Nanoparticles $Na_xAu_{25}(SC_2H_4Ph)_{18-y}(S(C_2H_4O)_5CH_3)_y$. *J. Am. Chem. Soc.* **2009**, *131*, 13844–13851.
93. Jobbins, M. M.; Raigoza, A. F.; Kandel, S. A. Adatoms at the Sulfur−Gold Interface in 1-Adamantanethiolate Monolayers, Studied Using Reaction with Hydrogen Atoms and Scanning Tunneling Microscopy. *J. Phys. Chem. C* **2011**, *115*, 25437–25441.
94. Rasband, W. S. *ImageJ*, http://rsb.info.nih.gov/ij/ (accessed June 1, 2009).